

Kulesh E. A., Piliptsov D. G., Rogachev A. V., Hong J. X., Fedosenko N. N.,  
Kolesnyk V. (2020). Boron-carbon coatings: structure, morphology and mechanical properties.  
*Journal of Engineering Sciences, Vol. 7(1), pp. C1–C9, doi: 10.21272/jes.2020.7(2).c1*

## Boron-Carbon Coatings: Structure, Morphology and Mechanical Properties

Kulesh E. A.<sup>1, 2\*</sup>, Piliptsov D. G.<sup>1, 2\*</sup> [0000-0001-5930-4066], Rogachev A. V.<sup>1, 2</sup> [0000-0001-8077-5954],  
Hong J. X.<sup>1</sup>, Fedosenko N. N.<sup>1, 2</sup>, Kolesnyk V.<sup>3</sup> [0000-0002-0417-3801]

<sup>1</sup> International Chinese-Belarusian Scientific Laboratory by Vacuum-Plasma Technologies,  
Nanjing University of Science and Technology, 200, Xiaolingwei St., 210094, Nanjing, China;

<sup>2</sup> Francisk Skorina Gomel State University, 104, Sovetskaya Street, 246019, Gomel, Belarus;

<sup>3</sup> Sumy State University, 2, Rymaskogo-Korsakova St., 40007, Sumy, Ukraine

### Article info:

Paper received:

June 14, 2020

The final version of the paper received:

September 28, 2020

Paper accepted online:

October 2, 2020

### \*Corresponding email:

v.kolesnik@tmvi.sumdu.edu.ua

**Abstract.** Boron-doped carbon coatings have been produced by a method combining the deposition of a pulsed carbon coating and a boron flow formed as a result of the evaporation of a boron target by pulsed YAG: Nd<sup>3+</sup> laser irradiation. Phase, chemical composition, structure, and mechanical properties of composite boron-carbon coatings have been determined. Changes in the coatings' roughness depending on the boron concentration have been established using atomic force microscopy. It has been shown that the grain size is on the rise with increasing boron concentration. Raman spectroscopy has revealed that at a boron concentration of 43.2 at. %. There is a sharp increase in the ID/IG ratio, which indicates the carbon component's graphitization. Low ID/IG ratios are observed in the coating at low boron concentrations (no more than 17.4 at. %), suggesting a high content of carbon atoms with sp<sup>3</sup> bond hybridization. The coating studies, carried out by X-ray photoelectron microscopy, showed that boron could be in a free state or in the form of carbide or oxide depending on the concentration in the coating. In this case, with an increase in boron concentration, there is a decrease in the concentration of carbon atoms in the state with sp<sup>3</sup> bond hybridization, accompanied by an increase in the number of B-C bonds and a reduction in the boron concentration not associated with carbon and oxygen. These coating and chemical composition features determine the boron concentration's established non-monotonic nature on their microhardness, elastic and mechanical properties.

**Keywords:** composite carbon coatings, boron-doped, atomic force microscopy, X-ray photoelectron microscopy, Raman spectroscopy, microhardness, scratch.

## 1 Introduction

The development of compositions, design and technological methods to produce hardening and protective coatings with high mechanical properties has always been an urgent challenge [1, 2]. As the said coatings, coatings based on amorphous carbon are widely used due to their high hardness and wear resistance. So, to reduce friction and wear, carbon coatings are deposited on bearing cages, gears, nozzles, and transmission components of machines and mechanisms [3–5]. Several types of such coatings have been developed. They are adapted in their properties to specific conditions and operating modes and provide a high service life under various modes and conditions of contact interaction [6–8], showing stable mechanical properties in specific temperature ranges [9, 10].

Carbon-based coatings (a-C), as noted, provide low values of the friction coefficient, as well as high wear resistance during friction with steel counter-surfaces [11]. The friction coefficient values usually vary from 0.01 to 0.5, depending on the coating's deposition method, structure, conditions, and test modes [12]. During frictional interaction in the contact area, the temperature rises [13], under the influence of which tribooxidative destruction occurs, which determines the destruction process of the coatings, and, as shown in [14], when the coating is destroyed, solid wear products in the friction zone activate the destruction of the counter body surface.

To create composite coatings, doping with elements such as silicon [15], fluorine [16] and nitrogen [17, 18], as well as metals: chromium [19] and titanium [19–21] is widely used. When metallic elements are included in the

structure of a-C coatings, as a rule, metal carbides are formed, distributed in the volume of the amorphous carbon matrix. It leads to a decrease in the stress-strain state of the coating, neutralizes the large difference in the mechanical parameters of the tool base and the coating [22]. Boron-doped carbon coatings are an object of broad interest among researchers for reasons related to both the specific properties of boron and the boron-carbon interaction. For example, in [23], the friction coefficient's low values characterize composite boron-carbon coatings in a friction couple with  $\text{Si}_3\text{N}_4$  compared to undoped carbon coatings. It was established that boron-carbon coatings, obtained by RF magnetron sputtering in a mixture of argon and  $\text{C}_2\text{H}_2$  showed high mechanical properties [24]. Their dependence on the hydrocarbon gas pressure, introduced in the sputtering process, and on the boron concentration was determined. In this case, however, it was not identified what had a predominant effect on the change in coating properties – the presence of hydrogen or boron.

For the carbon coatings obtained by physical sputtering of a graphite target, using a pulsed vacuum cathode discharge, there is a problem associated with the high fragility of the coatings, determined by high values of hardness and elastic modulus [25]. At high contact loads, under which elastic or plastic deformation of the substrate occurs, the resulting difference in elastic moduli between the coating and the substrate can cause an internal stress gradient with a maximum at the coating-substrate interface, which determines the destruction of the coating [22]. The abovementioned factors limit the use of a-C coatings only as functional elements of friction couples.

Considering high tribotechnical properties of bulk boron carbide and a-C coatings, to a certain extent mutually complementary, there is a motivation to form boron-doped a-C coatings with the properties characteristic of boron carbide while maintaining the properties of a carbon coating.

This paper aims at studying the features of the formation of boron-carbon coatings by the ion-plasma method, determining the effect of boron concentration on their structure, phase composition and mechanical properties.

## 2 Research Methodology

Boron-doped carbon coatings have been produced by a method combining the deposition of a pulsed carbon plasma coating and a boron flow formed as a result of the evaporation of a boron target by pulsed YAG:  $\text{Nd}^{3+}$  laser irradiation. To ensure maximum overlapping of plasma flows and uniformity of the distribution of the elements over the coating thickness, the substrates were placed at an angle of  $45^\circ$  to the graphite cathode axis of a pulsed cathode-arc carbon plasma source. A schematic of the experimental device is shown in Figure 1.

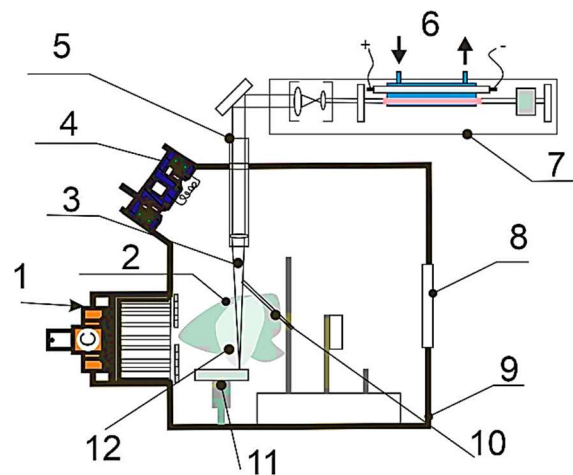


Figure 1 – Schematic of boron-carbon coatings deposition: 1 – pulse generator of carbon plasma; 2 – carbon plasma; 3 – laser beam; 4 – ion source; 5 – optical system inputs and focusing of laser radiation; 6 – laser cooling; 7-YAG:  $\text{Nd}^{3+}$  laser; 8 – window; 9 – chamber; 10 – substrate; 11 – the target of boron; 12 – the flow of boron

The thickness of the coatings was determined by the transverse cleavage using a scanning electron microscope (SEM) (Hitachi S-4800). Coatings of the same effective thickness of  $363 \pm 16$  nm were subjected to comparative analysis.

The surface morphology of the a-C:B composite coatings was studied using atomic force microscopy (AFM) in the topography and phase contrast measurement modes (Solver Pro, NT-MDT, Russia). The scanning field and scanning speed are  $10 \times 10 \mu\text{m}$  and  $1.0 \mu\text{m/s}$ , respectively.

The microstructure of the composite coatings was studied utilizing Raman spectroscopy. Raman spectra were excited by radiation with a length of 532 nm and a power of 20 mW (Senterra, Bruker).

The chemical composition and concentration of elements (Table 1) in the composite boron-carbon coating were determined using X-ray photoelectron spectroscopy (PHI quantera 2 XPS). The XPS spectra were excited by Al (K $\alpha$ ) cathode emission with energy of 1486.6 eV and a voltage of 15 kV. The exciting radiation power was 25 W. The spectrum was recorded from the surface area of the coating with a diameter of 100 micrometers. The binding energy in the XPS spectra was calibrated using the C1s line (284.6 eV).

The determination of the resulting coatings' mechanical properties was carried out using a Nanoscan 4D nanohardness tester. The measurements were performed in the dynamic mechanical analysis (DMA) mode.

Table 1 – Elemental composition of boron-doped carbon coatings

Coatings	$f_c$ , Hz	$f_L$ , Hz	C, at. %	B, at. %	O, at. %
$\alpha$ -C	10	–	97.6	–	2.4
$\alpha$ -C <sub>91.2</sub> :B <sub>2.3</sub>	10	5	91.2	2.3	6.5
$\alpha$ -C <sub>79.3</sub> :B <sub>17.4</sub>	10	33	79.3	17.4	3.3
$\alpha$ -C <sub>53.3</sub> :B <sub>43.2</sub>	10	50	53.3	43.2	3.5

$f_c$ , Hz – the frequency of the carbon plasma generator,  
 $f_L$ , Hz – laser pulse repetition rate

During measurement, harmonic oscillations with a frequency (20 Hz) and an amplitude of oscillations ( $\approx 3$ nm) are superimposed on the progressive implementation of the indenter [26], which causes a set of load-unload cycles. The values of elasticity modulus and hardness are calculated in each cycle. The maximum load was 40 mN. Thus, using this method, it is possible to determine the change in hardness and elasticity modulus with a depth resolution of 3 nm, i.e. to obtain practically continuous dependences of mechanical characteristics on depth [27]. Hardness and elasticity modulus are averaged values obtained as a result of 15 independent experiments.

The mechanical properties of the surface were diagnosed with the sclerometric method (Scratch Test) (WS-2005, China) was also used [18, 28]. The sclerometric tests [29, 30, 31].

The critical load ( $L_c$ ), at which the coating detachment from the substrate begins, is determined by the adhesive strength of the coating and substrate adhesion [32]. To assess the coating impact toughness, which characterizes the strength. The CPR<sub>s</sub> (crack propagation resistance) characteristic was used, calculated in according to the equation (1) [33]:

$$CPR_s = L_{c1} \times (L_{c2} - L_{c1}). \quad (1)$$

where  $L_{c1}$  is a load value at which crack initiation occurs,  $L_{c2}$  is a load value at which complete detachment of the coating from the substrate occurs [27, 34].

Plasticity characterizes a material's ability to absorb deformation energy during loading, distributing it over the crystal lattice or due to the formation of intergranular dislocations [35].

Tribological tests of the  $\alpha$ -C:B coatings, were carried out according to the "sphere-plane" scheme at a temperature of 23°C and relative humidity of 70%. A ball with a diameter of 5 mm was used as a counter body. The ball was made of hardened steel AISI 52100. The tests were conducted at a sliding speed of 0.0087 m/s, and a load of 0.98 N. After friction was carried out using an optical microscope, the diameter of the contact spot was determined, and the counter body volumetric wear coefficient was calculated using the following equation:

$$j = \frac{V}{FL} [m^3/N \cdot m], \quad (2)$$

where  $F$  is a load (N);  $L$  is a friction path (m);  $V$  is the volume of the spherical segment of the worn counter body material ( $m^3$ ).

### 3 Results and discussion

The studies carried out by scanning electron microscopy showed no defects such as pores and cracks on the surface and in the volume of deposited coatings. As well as there is no coating detachment from the substrate (Fig. 2), which indicates a high level of interphase interaction in the volume of the layer and on the boundary of the coating with the silicon substrate.

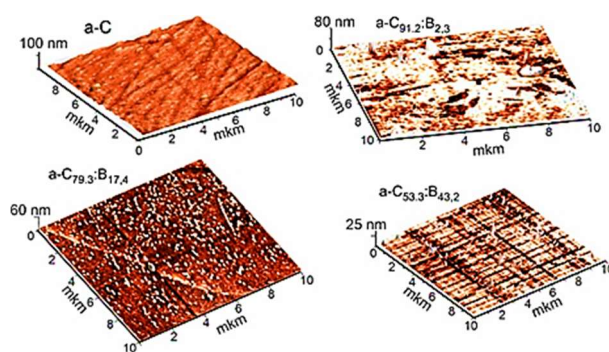


Figure 2 – AFM images of carbon coatings doped with different boron concentration

There are single large-sized grains on the surface of the  $\alpha$ -C<sub>79.3</sub>:B<sub>17.4</sub> coating, which is, as a rule, a droplet component of the flow and arise as a result of the evaporation of a graphite cathode by a pulsed arc. The  $\alpha$ -C<sub>91.2</sub>:B<sub>2.3</sub> coatings are characterized by higher heterogeneity. There are surface areas that are large enough with a relatively lower hardness than the rest of the areas. In general, composite coatings' morphology is more inhomogeneous compared to the  $\alpha$ -C coating and is characterized by higher values of the surface roughness  $R_a$  (Table 2).

Table 2 – Morphology parameters of  $\alpha$ -C:B coatings

Coatings	$R_a$ , nm	Average particle diameter $d$ , nm
$\alpha$ -C	2.4	7.6
$\alpha$ -C <sub>91.2</sub> :B <sub>2.3</sub>	6.2	12.3
$\alpha$ -C <sub>79.3</sub> :B <sub>17.4</sub>	2.2	26.4
$\alpha$ -C <sub>53.3</sub> :B <sub>43.2</sub>	7.2	23.2

According to AFM data (Table 2), the average size of surface particles, when introduced into the boron volume, increases and reaches a maximum value of 26.4 nm. Note that the coatings' surface morphology (roughness  $R_a$  and average grain size  $d$ ) depends on many conditions and is primarily determined by the coatings growth features. The presence of doping elements that can enter into chemical interaction with carbon, as well as the generation mode of carbon plasma, density and energy ion flow, which, according to the data of [11], determines the temperature of the substrate surface and leads to a change in the surface mobility of both carbon and boron atoms.

Doping of the  $\alpha$ -C coatings also leads to a change in their phase composition. Figure 3 shows the Raman spectra of the  $\alpha$ -C coatings with different boron

concentration. The shape of the Raman spectrum envelope of all coatings is characteristic of amorphous carbon coatings with varying hybridization types of carbon bonds. As can be seen, all spectra of boron – carbon coatings appear as a wide asymmetric peak in the range of 1000–2000  $\text{cm}^{-1}$ , which, according to [36, 37], contains information on  $\text{sp}^2$  hybridized carbon bonds, as well as on the degree of ordering and relative size  $\text{Csp}^2$  and  $\text{Csp}^3$  carbon clusters. The shape of the spectrum changes when the boron concentration in the coating increases. This shape is determined by the difference in the intensity ratio of D and G peaks, which indicates a change in the ratio of different carbon phases and the degree of orientation of carbon clusters in the coating. According to [37, 38], the change in the shape of the spectrum depends not only on the number and size of  $\text{Csp}^2$  and  $\text{Csp}^3$  clusters but also on the change in the angle of bonds between carbon and boron, which depends on the stoichiometry of boron carbide [39].

When the boron concentration is 2.3 at. %, the intensity ratio of D and G peaks practically does not change. Therefore, a low boron concentration does not affect the degree of ordering and the relative distribution of  $\text{Csp}^2/\text{Csp}^3$  of carbon phases in the coating. With increasing boron concentration in the coating, the intensity of D peak increases, and the G peak center's shift to the region of lower wavenumbers. For a highly boron-doped  $\alpha$ -C coating (Fig. 3) (boron concentration – 43.2 at.%), there is a significant change in the shape of the Raman spectrum, as well as an increase in the  $I_D/I_G$  ratio (Fig. 4).

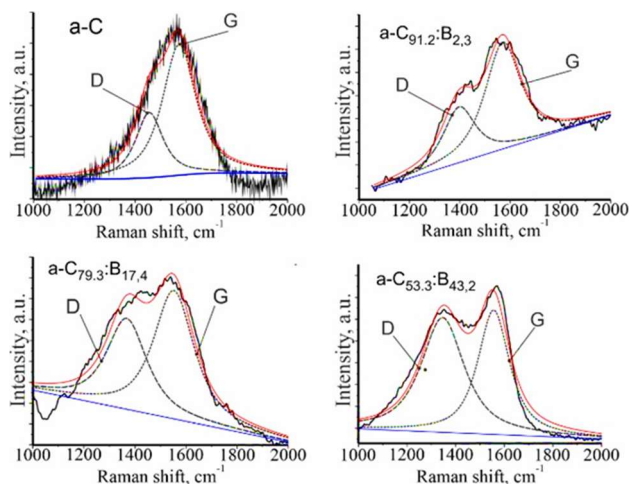


Figure 3 – Raman spectrum for the  $\alpha$ -C:B coating with different boron concentration

According to [40, 41], for  $\alpha$ -C coatings produced from pulsed flows of carbon plasma, the concentration of carbon atoms in the state with  $\text{sp}^3$  hybridized bonds increases with decreasing  $I_D/I_G$  value. In contrast, the coating is characterized by high mechanical properties provided that  $I_D/I_G \leq 1$ . It was shown in [20, 22] that an increase in the  $I_D/I_G$  ratio and a shift of the G peak to the region of lower wavenumbers in comparison with the peak position for the  $\alpha$ -C coating determine a decrease in the degree of structural ordering of  $\text{Csp}^3$  carbon clusters.

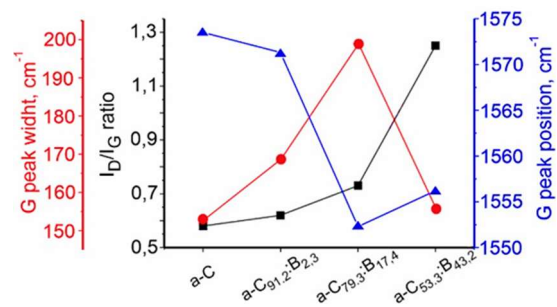


Figure 4 – Parameters of the Raman spectra of the  $\alpha$ -C:B coatings

Subsequently, it can be concluded that the shift in the G-peak position with a slight increase in the  $I_D/I_G$  ratio values, which is characteristic of the  $\alpha$ -C coatings with boron concentrations of 2.3 and 17.4 at. %, is determined by a change in the size and degree of ordering of  $\text{Csp}^3$  carbon clusters. Moreover, it was found in [40, 41] that an increase in the coating of carbon atoms in the state with  $\text{sp}^2$  hybridized bonds might be associated with the formation of C–B bonds in the coating. Boron predominantly interacts with carbon atoms with  $\text{sp}^3$  hybridized bonds, which leads to an increase in structural inhomogeneity, leading to a decrease in the degree of ordering of the carbon matrix, which is confirmed by the broadening of the G-peak of the Raman spectrum of the coatings. With an increase in the boron concentration, a further decrease in the coating  $\text{sp}^3$  bonds occurs.

The XPS spectra analysis of the  $\alpha$ -C and  $\alpha$ -C:B coatings showed oxygen besides carbon and boron (Fig. 5). The spectra of photoelectron states obtained with a high resolution and describing the chemical bonds characteristic of each element in the coating, namely the C1s peak (at 284.8 eV), the B1s (191 eV) and O1s (538 eV) peaks were subjected to further analysis [20, 21].

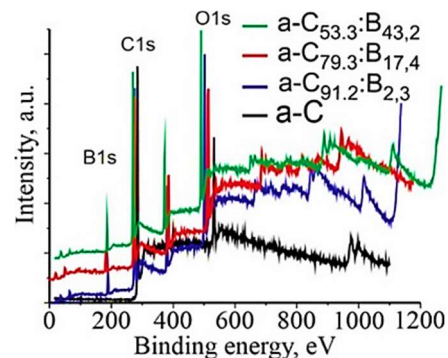


Figure 5 – XPS spectra of boron-carbon coatings with different boron concentration

Based on XPS data, it was defined that carbide compound of various stoichiometry is predominantly formed at a low boron concentration (2.3 at. %), but with a subsequent increase in boron concentration, the B-B component in the coating structure increases. At a high boron concentration (43.2 at. %), the structure of the carbon matrix is rearranged with the predominant presence of  $\text{Csp}^2$  and B-C phase volume. Such effect is associated

with the presence of more than one heterophase in the coating (carbon, carbide) [42, 43]. Quantity of heterophase forms the structure, as well as with chemical processes occurring in the volume of the coating leads to the formation of carbide compound and boron oxide compound on the coating surface. It was found that after the etching of the coating, a decrease in the bonds of B-O type is recorded, which confirms the assumption about the interaction of boron with oxygen after the depressurization of the vacuum chamber.

The results of processing the XPS spectra of energy states characteristic of carbon and boron (Figure 6). XPS spectra indicate that with an increase in the boron concentration in the coating, there is a decrease in the Csp<sup>3</sup> bonds of carbon atoms and a significant increase in the B-C bonds characteristic of boron carbide.

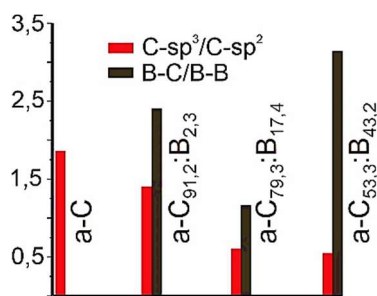


Figure 6 – Csp<sup>3</sup>/Csp<sup>2</sup> and B-C/B-B ratios in boron-carbon coatings

The data obtained by the XPS method are in agreement with the results of studying the structure of the coatings by Raman spectroscopy. It was concluded that the carbon structure is graphitized, and the degree of orientation of carbon Csp<sup>2</sup> clusters increased due to the boron binding to carbon atoms in the state with sp<sup>3</sup> bond hybridization. Thus, based on the results, it could be concluded that with an increase in the boron concentration in the coating structure, the content of Csp<sup>3</sup>-carbon clusters decreases due to their replacement by boron-carbon compounds of different stoichiometry.

Analyzing optical images of cracks on the coating surface after sclerometric testing (Figure 7), it is possible to divide the track into three stages, typical for various processes of coating destruction. In the first region (boundary Lc<sub>1</sub>), a crack is formed on the coating surface in the absence of lateral cracks arising in the direction perpendicular to the indenter displacement. The track profile is characterized by minimum width and a subtle print. At the second stage L<sub>C</sub> at a load from 7 to 14 N, the crack's width increases, and partial destruction of the coating surface is observed. At the third stage Lc<sub>2</sub>, the load reaches a critical value, i.e. complete detachment of the coating from the substrate and partial destruction of the substrate surface occur. The L<sub>C</sub> value, depending on the coating-base joint's adhesive strength, decreases with increasing boron concentration to 17.4 at. % and reaches maximum values of 20.5 N at high concentration.

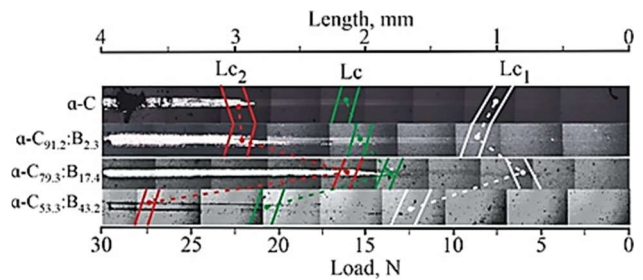


Figure 7 – Optical image of a crack on the α-C:B surface coating with different boron concentration

To analyze thin coatings' elastic properties, the so-called plasticity index is often used, which is defined as the ratio of hardness and elastic modulus (H/E) [27]. The H/E ratio, to some extent, characterizes the wear resistance of the coating [44]. After sclerometric tests (Fig. 7), according to equation (1), the CPR<sub>S</sub> values for the α-C:B coatings, obtained with different boron concentration, were determined (Table 4). It was found that the minimum CPR<sub>S</sub> value is characteristic for the α-C<sub>79.3</sub>:B<sub>17.4</sub> coating, which is consistent with the results of determining the H/E ratio for this coating. In this case, however, the CPR<sub>S</sub> α-C<sub>53.3</sub>:B<sub>43.2</sub> value of the coatings is significantly higher than for the coatings obtained at other boron concentration. Due to high residual stresses, which determine the high brittleness of the α-C coating (after sclerometric tests), a large number of microcracks are observed in the crack area (Fig. 7), which characterize the low adhesion of the α-C coating to the steel substrate. As shown in [22, 45], amorphous carbon coatings, depending on the deposition method, are characterized by high resistance to elastic deformation, and the H/E values are in the range of (0.08–0.20). Note that, according to [46, 47], the ratio value H/E ≈ 0.15 characterizes the “ideal elasticity” of the material and the high wear resistance of the coating [48]. The maximum values of CPR<sub>S</sub> (about 292) and H/E = 0.14 are characteristic for the α-C<sub>53.3</sub>:B<sub>43.2</sub> coatings. These values determine the high elastic properties of the coating and the ability to resist increasing loads.

Reduction of the critical load at boron concentrations of 2.3 and 17.4 at. % is associated with sp<sup>2</sup> clustering of the carbon matrix and high density of B-B and B-C bonds, which reduce the formation of C-C bonds. This leads to a decrease in hardness.

Table 4 – Mechanical properties of boron-carbon coatings

Coating	H, GPa	E, GPa	H/E	L <sub>C</sub> , N	CPR <sub>S</sub>
α-C	19.7 <sup>±3.8</sup>	210.5 <sup>±17.2</sup>	0.09	16.2	233.2
α-C <sub>91.2</sub> :B <sub>2.3</sub>	16.3 <sup>±1.6</sup>	120.5 <sup>±8.1</sup>	0.14	15.8	226.6
α-C <sub>79.3</sub> :B <sub>17.4</sub>	14.7 <sup>±1.3</sup>	110.4 <sup>±7.23</sup>	0.13	13.2	179.5
α-C <sub>53.3</sub> :B <sub>43.2</sub>	17.9 <sup>±1.6</sup>	124.7 <sup>±6.6</sup>	0.14	20.5	292.0

The hardness and modulus of the coatings' elasticity with different boron concentrations have been determined (Table 4). A decrease in the modulus of elasticity of doped coatings in comparison with undoped ones has been established. The decrease in hardness is determined by different ratios of Csp<sup>3</sup>/C-B phases in coatings with different boron concentration and a change in the size of carbon clusters.

At a low boron concentration, there is a decrease in hardness, which is determined by structural defects and increasing in the misorientation degree of carbon clusters. With an increase in the size of the clusters of the carbon matrix, according to the Hall-Petch law, there is an increase in intergranular slip. It leads to a decrease in microhardness due to the presence of a large number of defects at grain boundaries [49]. At a boron concentration of 2.3 at. Hardness is mainly determined by the carbon matrix, particularly by the size and packing of  $C_{sp^2}$  and  $C_{sp^3}$  carbon clusters. At a boron concentration of more than 17.3 at.%, boron and the degree of its chemical interaction with carbon have a predominant effect on the microhardness. According to XPS data, a high boron concentration of carbide compounds is formed, which leads to an increase in the coating hardness and an increase in the elastic modulus. A slight decrease in microhardness for the  $\alpha-C_{53,3}:B_{43,2}$  coatings containing a high concentration of C-B compounds is determined by the effect of oxide compounds on the coating surface [50].

Thus, by the results of structure analysis, it is confirmed that a decrease in the hardness of the  $\alpha-C:B$  composite coating may be associated with the rearrangement of graphite bonds due to the introduction of B atoms. It was established that the introduction of boron atoms or boron-based compounds into the structure of carbon coatings makes it possible to change the hardness and modulus of elasticity and the kinetics of friction and wear of the counter body (Figure 8–9). At the initial stage of friction, high values of the friction coefficient are observed, which are characteristic of a friction couple's running-in area and stable contact formation. The width of the running-in zone, as a rule, depends on the surface roughness and on its hardness, the intensity of graphitization processes in the contact zone [3]. The presence of a wide running-in area is typical for the  $\alpha-C_{53,3}:B_{43,2}$  coatings. After reaching a stationary friction mode, a decrease in the friction coefficient is observed for values typical for  $\alpha-C$  coatings. Such effect is associated with a change in the surface and volumetric structure of the coating and an increase in the surface's elastic properties due to the presence of B-C bonds (Figure 9). A higher coefficient of the counterbody wear during friction with the  $\alpha-C_{53,3}:B_{43,2}$  coating is determined by higher surface roughness ( $R_a=22.3$  nm) of the coating.

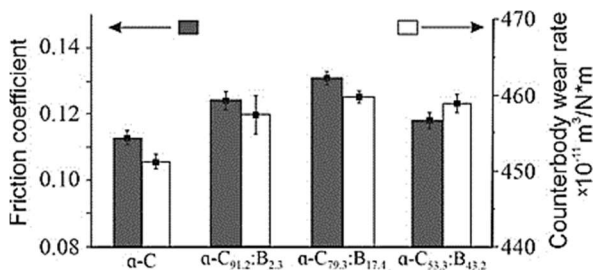


Figure 8 – Values of the volumetric wear of the counterbody and the friction coefficient

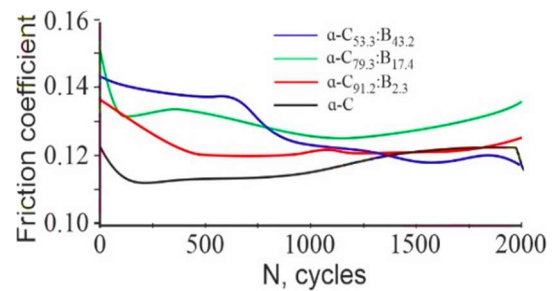


Figure 9 – Change of friction coefficient during the friction of the  $\alpha-C:B$  coatings

When a boron concentration in the coating is 42.3 at. % (Figs. 8, 9), a large width of the running-in area is observed, which characterizes the friction coefficient about 0.14. After 1000 friction cycles, the friction coefficient decreases to values typical for undoped  $\alpha-C$  coatings in the stationary friction mode. The friction kinetics of boron-doped carbon coatings is similar to the friction kinetics of the  $\alpha-C:Si$  coatings, and consists in the occurrence of trioxidation reactions in the contact area, leading to the formation of oxide compounds, such as B-O, which forms a transit boundary layer. As shown above, boron oxidation might occur during coating deposition due to interaction with residual oxygen in the vacuum chamber or during interaction with oxygen at depressurization of the vacuum chamber.

#### 4 Conclusions

The features of the formation of boron-carbon coatings by the ion-plasma method, the regularities of the boron concentration effect on their structure, phase composition, and mechanical properties have been determined. With the SEM method, it was found that the formation of a granular structure is characteristic of  $\alpha-C:B$  coatings, the parameters of which non-monotonically depend on the boron concentration. Raman spectroscopy was used to analyze the change in the carbon matrix's phase composition while doping with boron. It is shown that at a boron concentration of 43.2 at. %. There is a sharp increase in the  $I_D/I_G$  ratio, which indicates the carbon component's graphitization. At a boron concentration of 2.3 and 17.4 at. % in the coating, low values of the  $I_D/I_G$  ratio are recorded, which suggests a high content of carbon atoms with  $sp^3$  bond hybridization. The XPS method shows that, depending on the coating's boron concentration, boron can be found either in the form of carbide, boron oxide, or in the form of a separate phase. It is found that with increasing boron concentration, the concentration of carbon atoms in the state with  $sp^3$  bond hybridization decreases, accompanied by an increase in the concentration of B-C bonds and a decrease in the amount of pure boron. This behavior allows concluding that boron interacts with carbon atoms at high concentrations in the state of  $sp^3$  bond hybridization.

Microhardness and modulus of elasticity of coatings with different boron concentrations have been determined. A decrease in the modulus of elasticity of doped carbon

coatings compared with undoped ones has been established.

Critical loads of coatings destruction ( $L_C$ ) have been determined using sclerometry. The  $L_C$  value, depending on the value of the coating adhesive interaction with the substrate, decreases with an increase in the boron concentration to 17.4 at. % and reaches maximum values of 20.5 N at high concentration. The dependence of the crack propagation resistance ( $CPR_S$ ) on the boron concentration is shown. The maximum  $CPR_S$  values have been found to be characteristic of the a-C coating doped with boron with a concentration of 43.2 at. %.

The ambiguous nature of the boron concentration influence is also manifested in the study of doped coatings' mechanical properties. The friction coefficient varies from 0.12 to 0.15 while maintaining a relatively low coefficient of the counterbody wear during friction, which, together

with the data on mechanical parameters, determines the high efficiency of using doped coatings as antifriction ones.

## 5 Acknowledgments

Intergovernmental Cooperation Projects supported this work in the National Key Research and Development Plan of the Ministry of Science and Technology of PRC (projects No. 2016YFE0111800), task 3.4.23 "Synthesis of high-alloyed boron and their compounds coatings from amorphous carbon, determination of their structural and phase bonds, mechanical and corrosion properties during operation in the environment of fuels and oils performed by SPRI "Physical materials science, new materials and technologies" (Republic of Belarus).

## References

1. Nakazawa, H., Sudoh, A., Suemitsu, M., Yasui, K., Itoh, T., Endoh, T., Narita Y. Mashita, M. (2010). Mechanical and tribological properties of boron, nitrogen-coincorporated diamond-like carbon films prepared by reactive radio-frequency magnetron sputtering. *Diamond and Related Materials*, Vol. 19(5), pp. 503–506, doi:10.1016/j.diamond.2010.01.026.
2. He, D., Shang, L., Lu, Z., Zhang, G., Wang, L., Xue, Q. (2017). Tailoring the mechanical and tribological properties of B<sub>4</sub>C/a-C coatings by controlling the boron carbide content. *Surface and Coatings Technology*, Vol. 329, pp. 11–18, doi:10.1016/j.surfcoat.2017.09.017.
3. Donnet, C. (1998). Recent progress on the technology of doped diamond-like and carbon alloy coatings. *Surface and Coatings Technology*, Vol. 100, pp.180–186, doi.org/10.1016/S0257-8972(97)00611-7.
4. Cuong, P. D., Ahn, H.-S., Yoon, E.-S., Shin, K.-H. (2006). Effects of relative humidity on tribological properties of boron carbide coating against steel. *Surface and Coatings Technology*, Vol. 201(7), pp. 4230–4235, doi:10.1016/j.surfcoat.2006.08.093.
5. Wentorf, R.H. (1961). Synthesis of the Cubic Form of Boron Nitride. *The Journal of Chemical Physics*, Vol. 34, pp. 809, doi.org/10.1063/1.1731679.
6. Solozhenko, V. L., Andrault, D., Fiquet, G., Mezouar, M., Rubie, D. C. (2001). Synthesis of superhard cubic BC<sub>2</sub>N. *Applied Physics Letters*, Vol. 78(10), pp. 1385–1387, doi:10.1063/1.1337623.
7. Cordero, B., Gómez, V., Platero-Prats, A. E., Revés, M., Echeverría, J., Cremades, E., Barragan, F., Alvarez, S. (2008). Covalent radii revisited. *Dalton Transactions*, Vol. 21, pp. 2832–2838, doi:10.1039/b801115j.
8. Ito, H., Hori, K., Saitoh, H. (2006). Deposition of mechanically hard amorphous carbon nitride films from decomposition of BrCN. Effects of substrate cooling and pulsed rf-bias voltage. *Journal of Non-Crystalline Solids*, Vol. 352(1), pp.1–7, doi.org/10.1016/j.jnoncrysol.2005.11.015.
9. Kleinsorge, B., Ferrari, A. C., Robertson, J., Milne, W. I. (2000). Influence of nitrogen and temperature on the deposition of tetrahedrally bonded amorphous carbon. *Journal of Applied Physics*, Vol. 88(2), pp. 1149–1157, doi:10.1063/1.373790 1149.
10. Mori, H., Tohyama, M., Okuyama, M., Ohmori, T., Ikeda, N., Hayashi, K. (2017). Low Friction Property of Boron Doped DLC under Engine Oil. *Tribology Online*, Vol. 12(3), pp. 135–140, doi:10.2474/trol.12.135.
11. Sikora, A., Berkesse, A., Bourgeois, O., Garden, J.-L., Guerret-Piécourt, C., Rouzaud, J.-N., Loir, A.-S., Garrelie, F., Donnet, C. (2009). Structural and electrical characterization of boron-containing diamond-like carbon films deposited by femtosecond pulsed laser ablation. *Solid State Sciences*, Vol. 11(10), pp. 1738–1741, doi:10.1016/j.solidstatesciences.2008.07.013.
12. Liza, S., Ohtake, N., Akasaka, H., Munoz-Guijosa, J. M. (2015). Tribological and thermal stability study of nanoporous amorphous boron carbide films prepared by pulsed plasma chemical vapor deposition. *Science and Technology of Advanced Materials*, Vol. 16(3), pp. 035007, doi:10.1088/1468-6996/16/3/035007.
13. Liza, S., Hieda, J., Akasaka, H., Ohtake, N., Tsutsumi, Y., Nagai, A., Hanawa, T. (2017). Deposition of boron doped DLC films on TiNb and characterization of their mechanical properties and blood compatibility. *Science and Technology of Advanced Materials*, Vol. 18(1), pp. 76–87, doi:10.1080/14686996.2016.1262196 87.
14. Ming, M. Y., Piliptsov, D. G., Rudenkov, A. S., Rogachev, A. V., Jiang, X., Dongping, S., Chaus, A. S., Balmakou, A. (2017). Structure, mechanical and tribological properties of Ti-doped amorphous carbon films simultaneously deposited by magnetron sputtering and pulse cathodic arc. *Diamond and Related Materials*, Vol. 77, pp. 1–9, doi.org/10.1016/j.diamond.2017.05.010.
15. Chaus, A. S., Jiang, X. H., Pokorný, P., Piliptsov, D. G., Rogachev, A. V. (2018.) Improving the mechanical property of amorphous carbon films by silicon doping. *Diamond and Related Materials*, Vol. 82, pp. 137–142, doi.org/10.1016/j.diamond.2018.01.013.

16. Wang, J., Ma, J., Huang, W., Wang, L., He, H., Liu, C. (2017). The investigation of the structures and tribological properties of F-DLC coatings deposited on Ti-6Al-4V alloys. *Surface and Coatings Technology*, Vol. 316, pp. 22–29, doi.org/10.1016/j.surfcoat.2017.02.065.
17. Piliptsov, D. G., Rogachev, A. A., Chizhik, S. A., Rudenkov, A. S., Kulesh, E. A., Fedosenko, N. N. (2018). Phase composition and structure of multilayer nanosized metalcarbon coatings. *PFMT*, Vol. 2(35), pp. 34–37.
18. Zhou, B., Jiang, X., Rogachev, A. V., Sun, D., Zang, X. (2013). Growth and characteristics of diamond-like carbon films with titanium and titanium nitride functional layers by cathode arc plasma. *Surface and Coatings Technology*, 223, 17–23. doi:10.1016/j.surfcoat.2013.02.020.
19. Rogachev, A. V., Rudenkov, A. S., Piliptsov, D. G., Jiang, X., Fedosenko, N. N. (2017). Phase Composition, Structure and Mechanical Properties of Carbon Coatings Doped by Carbide-Forming Metals. *Recent Advances in Technology Research and Education*, pp. 18–25. doi:10.1007/978-3-319-67459-9\_3.
20. Zhou, B., Liu, Z., Rogachev, A. V., Piliptsov, D. G., & Tang, B. (2016). Size effect in the titanium/diamond-like carbon bilayer films: effect of relative thickness on their structure and mechanical properties. *Surface and Interface Analysis*, Vol. 49(1), pp. 47–54, doi:10.1002/sia.6056.
21. Zhou, Y., Li, L., Shao, W., Chen, Z., Wang, S., Xing, X., & Yang, Q. (2020). Mechanical and tribological behaviors of Ti-DLC films deposited on 304 stainless steel: Exploration with Ti doping from micro to macro. *Diamond and Related Materials*, Vol. 107, pp. 107870, doi:10.1016/j.diamond.2020.107870.
22. Charitidis, C.A. (2010). Nanomechanical and nanotribological properties of carbon-based thin films: a review, *International Journal of Refractory Metals and Hard Materials*, Vol. 28, pp. 51–70, doi.org/10.1016/j.ijrmhm.2009.08.003.
23. Xu, F., Yuen, M. F., He, B., Wang, C. D., Zhao, X. R., Tang, X. L., Zuo, D. W., Zhang, W. J. (2014). Microstructure and tribological properties of cubic boron nitride films on Si<sub>3</sub>N<sub>4</sub> inserts via boron-doped diamond buffer layers. *Diamond and Related Materials*, Vol. 49, pp. 9–13, doi:10.1016/j.diamond.2014.07.014.
24. Ren, Z., Qin, H., Dong, Y., Doll, G. L., Ye, C. (2019). A boron-doped diamond like carbon coating with high hardness and low friction coefficient. *Wear*, Vol. 436, pp. 203031, doi:10.1016/j.wear.2019.203031.
25. Zavaleyev, V., Walkowicz, J., Greczynski, G., Hultman, L. (2013). Effect of substrate temperature on properties of diamond-like films deposited by combined DC impulse vacuum-arc method. *Surface and Coatings Technology*, Vol. 236, pp. 444–449, doi:10.1016/j.surfcoat.2013.10.023.
26. Menard, K. P., Menard, N. (2017). Dynamic Mechanical Analysis. *Encyclopedia of Analytical Chemistry*, pp. 1–25, doi:10.1002/9780470027318.a2007.pub3.
27. Dwivedi, N., Kumar, S. (2012). Nanoindentation testing on copper/diamond-like carbon bi-layer films. *Current Applied Physics*, Vol. 12(1), pp. 247–253, doi:10.1016/j.cap.2011.06.013.
28. Wang, P., Wang, X., Xu, T., Liu, W., Zhang, J. (2007). Comparing internal stress in diamond-like carbon films with different structure. *Thin Solid Films*, Vol. 515(17), pp. 6899–6903, doi:10.1016/j.tsf.2007.02.069.
29. Zhang, S., Sun, D., Fu, Y., Du, H. (2005). Toughening of hard nanostructural thin films: a critical review. *Surface and Coatings Technology*, Vol. 198(1), pp. 2–8, doi:10.1016/j.surfcoat.2004.10.020.
30. Robertson, J. (1991). Hard amorphous (diamond-like) carbons. *Progress in Solid State Chemistry*, Vol. 21, pp. 199–333, doi.org/10.1016/0079-6786(91)90002-H.
31. Cemin, F., Bim, L. T., Menezes, C. M., Maia da Costa, M. E. H., Baumvol, I. J. R., Alvarez, F., Figueroa, C. A. (2015). The influence of different silicon adhesion interlayers on the tribological behavior of DLC thin films deposited on steel by EC-PECVD. *Surface and Coatings Technology*, Vol. 283, pp. 115–121, doi:10.1016/j.surfcoat.2015.10.031.
32. Barshilia, H. C., Ananth, A., Khan, J., Srinivas, G. (2012). Ar + H<sub>2</sub> plasma etching for improved adhesion of PVD coatings on steel substrates. *Vacuum*, Vol. 86(8), pp. 1165–1173, doi:10.1016/j.vacuum.2011.10.028.
33. Attar, F., Johannesson, T. (1996). Adhesion evaluation of thin ceramic coatings on tool steel using the scratch testing technique. *Surface and Coatings Technology*, Vol. 78(1-3), pp. 87–102, doi:10.1016/0257-8972(94)02396-4.
34. Wang, A.-Y., Lee, K.-R., Ahn, J.-P., Han, J. H. (2006). Structure and mechanical properties of W incorporated diamond-like carbon films prepared by a hybrid ion beam deposition technique. *Carbon*, Vol. 44(9), pp. 1826–1832, doi:10.1016/j.carbon.2005.12.04.
35. Gayathri, S., Kumar, N., Krishnan, R., Ravindran, T. R., Dash, S., Tyagi, A. K., Sridharan, M. (2015). Influence of Cr content on the micro-structural and tribological properties of PLD grown nanocomposite DLC-Cr thin films. *Materials Chemistry and Physics*, Vol. 167, pp. 194–200, doi:10.1016/j.matchemphys.2015.10.031.
36. Zhang, L. L., Yang, Q., Tang, Y., Yang, L., Zhang, C., Hu, Y., Cui, X. (2015). Synthesis and characterization of boron incorporated diamond-like carbon thin films. *Thin Solid Films*, 589, 457–464. doi:10.1016/j.tsf.2015.05.067.
37. Tan, M., Zhu, J., Han, J., Gao, W., Liu, A., Han, X. (2008). Raman characterization of boron doped tetrahedral amorphous carbon films. *Materials Research Bulletin*, Vol. 43(2), pp. 453–462, doi:10.1016/j.materresbull.2007.02.037.
38. Dai, W., Ke, P., Wang, A. (2011). Microstructure and property evolution of Cr-DLC films with different Cr content deposited by a hybrid beam technique. *Vacuum*, Vol. 85(8), pp. 792–797, doi:10.1016/j.vacuum.2010.11.013.
39. Fan, D., Lu, S., Guo, Y., Hu, X. (2018). Two-dimensional stoichiometric boron carbides with unexpected chemical bonding and promising electronic properties. *Journal of Materials Chemistry C*, Vol. 6(7), pp. 1651–1658, doi:10.1039/c7tc04505k.

40. Jana, D., Sun, C.-L., Chen, L.-C., Chen, K.-H. (2013). Effect of chemical doping of boron and nitrogen on the electronic, optical, and electrochemical properties of carbon nanotubes. *Progress in Materials Science*, Vol. 58(5), pp. 565–635, doi:10.1016/j.pmatsci.2013.01.003.
41. Chhowalla, M., Yin, Y., Amaratunga, G. A. J., McKenzie, D. R., Frauenheim, T. (1996). Highly tetrahedral amorphous carbon films with low stress. *Applied Physics Letters*, Vol. 69(16), pp. 2344–2346, doi:10.1063/1.117519.
42. Wang, X., Zhao, Y. (2015). Study of Electrical Conductivity and Microcosmic Structure of Tetrahedral Amorphous Carbon Films Doped by Boron. *Advances in Materials Science and Engineering*, Vol. 2015, pp. 1–6, doi:10.1155/2015/727285.
43. Tamura, Y., Zhao, H., Wang, C., Morina, A., Neville, A. (2016). Interaction of DLC and B4C coatings with fully fated oils in boundary lubrication conditions. *Tribology International*, Vol. 93, pp. 666–680, doi:10.1016/j.triboint.2015.02.029.
44. Zou, C. W., Wang, H. J., Feng, L., Xue, S. W. (2013). Effects of Cr concentrations on the microstructure, hardness, and temperature-dependent tribological properties of Cr-DLC coatings. *Applied Surface Science*, Vol. 286, pp. 137–141, doi:10.1016/j.apsusc.2013.09.036.
45. Choi, W. S., Heo, J., Chung, I., Hong, B. (2005). The effect of RF power on tribological properties of the diamond-like carbon films. *Thin Solid Films*, Vol. 475(1), pp. 287–290, doi:10.1016/j.tsf.2004.07.033.
46. Leyland, A., Matthews, A. (2000). On the significance of the H/E ratio in wear control: a nanocomposite coating approach to optimised tribological behaviour. *Wear*, Vol. 246(1), pp. 1–11, doi:10.1016/s0043-1648(00)00488-9.
47. Lawn, B. R., Howes, V. R. (1981). Elastic recovery at hardness indentations. *Journal of Materials Science*, Vol. 16(10), pp. 2745–2752, doi:10.1007/bf00552957.
48. Oliver, W. C., Pharr, G. M. (2004). Measurement of hardness and elastic modulus by instrumented indentation: Advances in understanding and refinements to methodology. *Journal of Materials Research*, Vol. 19(01), pp. 3–20, doi:10.1557/jmr.2004.19.1.3.
49. Hansen, N. (2004). Hall–Petch relation and boundary strengthening. *Scripta Materialia*, Vol. 51(8), pp. 801–806, doi:10.1016/j.scriptamat.2004.06.002.
50. Kang, X., Zhang, Z., Gou, L. (2020). Improvement in Electrical Conductivity of Boron-doped Diamond Films after Hydrogen Plasma and Vacuum Heat Treatment. *Applied Surface Science*, Vol. 526, pp. 1–27, doi.org/10.1016/j.apsusc.2020.146738.